32nd Annual International Conference of the IEEE EMBS
Buenos Aires, Argentina, August 31 - September 4, 2010

Targeting Error Simulator for Image-guided Prostate Needle Placement

Andras Lasso, *Member,* Shachar Avni, and Gabor Fichtinger, *Member, IEEE*

***Abstract*—Motivation: Needle-based biopsy and local therapy of prostate cancer depend multimodal imaging for both target planning and needle guidance. The clinical process involves selection of target locations in a pre-operative image volume and registering these to an intra-operative volume. Registration inaccuracies inevitably lead to targeting error, a major clinical concern. The analysis of targeting error requires a large number of images with known ground truth, which has been infeasible even for the largest research centers. Methods: We propose to generate realistic prostate imaging data in a controllable way, with known ground truth, by simulation of prostate size, shape, motion and deformation typically encountered in prostatic needle placement. This data is then used to evaluate a given registration algorithm, by testing its ability to reproduce ground truth contours, motions and deformations. The method builds on statistical shape atlas to generate large number of realistic prostate shapes and finite element modeling to generate high-fidelity deformations, while segmentation error is simulated by warping the ground truth data in specific prostate regions. Expected target registration error (TRE) is computed as a vector field. Results: The simulator was configured to evaluate the TRE when using a surface-based rigid registration algorithm in a typical prostate biopsy targeting scenario. Simulator parameters, such as segmentation error and deformation, were determined by measurements in clinical images. Turnaround time for the full simulation of one test case was below 3 minutes. The simulator is customizable for testing, comparing, optimizing segmentation and registration methods and is independent of the imaging modalities used.**

I. Introduction

Prostate cancer continues to be a worldwide health problem. The biopsy and localized therapy of prostate cancer involves needle placement under image guidance. The typical workflow begins with extensive pre-operative (pre-op) diagnostic imaging and based on these images the biopsy or therapy target locations are identified. During the procedure, intra-operative (intra-op) images are acquired to determine the current position of the planned targets and then to verify the accuracy of needle placement relative to the target anatomy. Transforming pre-op targets into intra-op imagery is a supremely difficult task, due to incessant organ deformation, dislocation, and inherent differences between the pre-op and intra-op imaging modalities. A substantial arsenal of methods has been developed to register pre-op and intra-op prostate images, involving just about all combinations of popular prostate imaging modalities: ultrasound, MRI, CT, and cone beam fluoroscopy. Validation and quantitative comparison of the competing approaches require a large number of images with known ground truth for prostate and internal target locations. Acquiring lots of high- quality clinical images is prohibitively expensive and, more often than not, infeasible intra-operatively. In short, despite decades of research in image-guided surgery, ground truth target dislocation information in clinical imagery is virtually nonexistent. Even under the very best of circumstances, information is limited to surrogates, such as manually segmented contours and anatomical landmarks. The overarching goal of our project is to create a simulation environment to generate realistic prostate imaging data in a controllable way, with known ground truth, with the primary purpose of serving the evaluation, comparison, and optimization of target registration methods, specifically in image-guided prostate interventions. Recent studies of target registration error (TRE) in prostate needle placement involved MRI-to-MRI [1] and MRI-to-ultrasound [2] registration. Like earlier studies, these too were carried out on limited amount and loosely controlled clinical data, typically involving a few dozen or so patients, owing to difficulties in acquiring patient data with trustable reference information regarding the planned and achieved target locations.

Physics-based simulation environments could produce large amounts of high-fidelity prostate data with known target location ground truth. Misra *et al.* [3] created Finite Element Model (FEM) of the prostate and surrounding structures (bladder, pubic bone, rectum, urethra, as well as different abdominal tissues). Goksel *et al*. [4] also used FEM for simulating needle-tissue interaction in the prostate. Hensel *et al*. [5] and Courtis *et al*. [6] reported an FEM-based method for registering MRI images for radiotherapy planning and detecting prostate tissue abnormalities.

Lee *et al.* [7] used FEM-based simulation for registration validation. They applied a complex set of boundary conditions, which may result in a highly realistic deformation field simulation. However, for many applications a simpler model could be sufficient, and the described method requires actual patient images with multiple segmented organs, which may be prohibitive if a large number of test data sets are needed.

Our contribution is twofold. We designed and implemented a highly customizable simulator for TRE evaluation of 3D prostate image registrations. We employ finite element modeling to generate realistic test cases with ground truth. Different registration methods can be tested

Manuscript received April 23, 2010. This work has been supported by the National Institute of Health under grants 5R01CA111288-04 and 5R01EB002963-05.

Andras Lasso, Shachar Avni, and Gabor Fichtinger are with the School of Computing, Queen's University, Kingston, Canada K7L3N6 (email: lasso@cs.queensu.ca, savni@cs.queensu.ca, gabor@cs.queensu.ca)

with defining prostate shape variability, deformation, and segmentation error. Secondly, as a way of testing, we configured the simulator to investigate a pertinent clinical question. It was posited that in MR-guided robotic prostate biopsy, observed prostate deformations and segmentation errors in surface-based target registration usually does not manifest in clinically significant target registration error in relevant biopsy locations.

II. Methods

The objective of the proposed simulator is to evaluate targeting error while using image registration methods developed to compensate organ motion and deformation. The workflow, shown in Fig. 1, begins with generating a ground truth pre-operative prostate shape (*pre-op image*). Deformation of the *pre-op image* is then simulated by Finite Element Analysis (FEA) that provides the ground truth intra-operative image (*intra-op image*) and a dense deformation field for the whole prostate volume (*ground truth deformation field*). Next, *pre-op* and *intra-op image* segmentation is simulated by applying typical errors to the ground truth segmentation. The segmented contours are then aligned using the registration method that is to be evaluated. The output of the registration is a dense deformation field (*reconstructed deformation field*), constructed from the found optimal transform. Finally, the difference between the *reconstructed* and *ground truth deformation fields* is computed to obtain the TRE for each voxel position in the *pre-op image*.

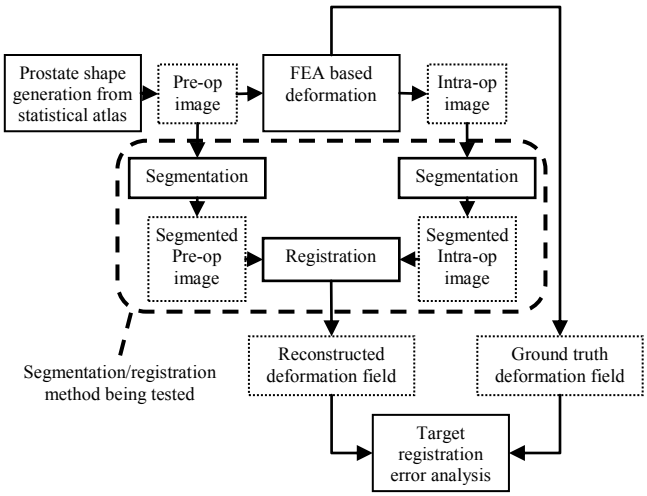

Fig. 1. Simulation workflow for evaluating TRE on a single dataset.

A. Generation of 3D prostate contours with a statistical shape atlas

One important requirement of the simulator is the ability to generate a large number of test cases given a finite number of sample input data. Using the method described by Tsai *et al*. [8], we obtained and aligned a set of 3D prostate contours, constructed from stacks of segmented axial slices and modeled as voxelized binary volumes. From this set, we obtained the mean shape and three eigenshapes, using the technique developed by Leventon *et al*. [9]. We then obtained the prostate contour by adding the weighted average of the eigenshapes to the mean shape. The weights for averaging were randomly generated from within the corresponding eigen-value bounds. The contour is then converted to a surface mesh and smoothed (by using the marching cubes algorithm, and a windowed sinc function interpolation kernel, respectively). The resulting surface mesh is used as input for the finite element volumetric mesh generation.

B. Deformation using Finite Element Analysis

A realistic and dense deformation field is required for accurately computing the dislocation of all potential target points in the prostate, which can be achieved by using finite element analysis. We built our finite element model from two objects: *prostate* and *body* (Fig. 2.) The *prostate* object represents the prostate gland, and the *body* object simulates the pelvic soft tissues supporting the prostate. *Prostate* was constructed by filling the atlas-generated surface mesh with tetrahedral elements. *Body* was modeled as an 80 mm diameter sphere around the *prostate* object, and also filled with tetrahedral elements. We used the open source *Netgen* library (Johannes Kepler University Linz, available at www.hpfem.jku.at/netgen) for the volumetric mesh construction, for its ability to rapidly generate a simple, smooth, high-quality volumetric mesh suitable for FEA.

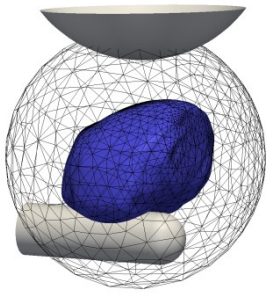

Fig. 2. Sample geometry of the *prostate* (solid surface in the middle) and the *body* object (wireframe sphere around the prostate). Force is applied on *body* mesh nodes that lie within the cylindrical shape of the endorectal probe. Position of the anterior side of the *body* object (at the top, intersection with the solid sphere part) is fixed.

Material model and properties were adapted from [6]; both objects are modeled as linear elastic materials, *prostate* with Poisson ratio $v = 0.4$ and Young's modulus $E = 21$ kPa, *body* with $v = 0.4$ and Young's modulus $E = 15$ kPa.

Loads and boundary conditions determine the forces that dislocate and deform the objects. We chose to simulate a clinically pertinent scenario: the deformation caused by patient motion during transrectal robot-assisted biopsy. The end-effector of the robot is inserted into the rectum and then it is fixed to the table. During the procedure, patients tend to move slightly in order to reduce their discomfort, and as a result the robot's end-effector applies strong local pressure on the prostate, causing considerable dislocation and deformation. We modeled this setup by prescribing force

loads (with random perturbations in orientation and magnitude) on the mid-posterior surface of the prostate. To avoid rigid-body translation we added fixed position constraint on the *body* object mesh nodes on its anterior side. The *prostate* and *body* meshes are created separately to maintain a smooth boundary surface, so we had to add a boundary condition to tie the outer surface of the *prostate* with the inner surface of the *body*. All the prostate models are generated by the same atlas, thus they are inherently aligned and the same boundary conditions apply to all prostate model instances.

We perform a quasi-static analysis using the open source FEBio solver (developed at the Scientific Computing and Imaging Institute at the University of Utah, www.sci.utah.edu/software) to compute the prostate deformation from the above described geometry, material, and boundary condition model.

C. Segmentation simulation

The goal of this step is to simulate errors of a realistic segmentation algorithm. This allows the evaluation of the segmentation error effect on the final TRE for surface-based registration methods.

The segmentation simulation inputs are the ground truth segmented image and a segmentation error model. The segmentation error model describes the segmentation error in one or more regions of the prostate, reflecting where and what kind of segmentation errors typically occur (e.g., under-segmentation in the apex region in case of manual segmentation, or leaking of the prostate into the bladder in case of a gradient-based automatic segmentation method).

The inputs of the segmentation error simulator are the ground truth image and multiple error regions (each defined with the maximum error position, error vector, and influenced region size). For each error region a dense deformation field is generated by a cubic B-spline interpolator, and then these deformations are subsequently applied on the input image to produce the simulated segmented image.

D. Registration

The simulated segmented *pre-op* and *intra-op images* are registered to compute a transform between positions in the two image spaces. The transform is then evaluated for all voxels of the *intra-op* image to get the *reconstructed deformation* field. This deformation field is directly comparable to the ground truth deformation field, as they are both defined in the *intra-op* image space.

A practical goal of the simulation framework was to evaluate applicability of rigid registration to estimate target displacement resulting from non-rigid prostate deformation. Therefore, we used a simple rigid registration method for our current tests (with rigid translation with versor rotation transform, mean squares metrics, and gradient descent optimizer). Other registration algorithms that work with segmented images and can produce a dense deformation field could be used without any change in the simulator (to evaluate the accuracy and robustness of a registration method or optimize registration parameters, etc.). Testing image-based registration algorithms is also possible, but it requires modification of the shape generation step (e.g., to accept image contours as input, instead of generating it from an atlas).

E. Target registration error evaluation

The goal of this step is to analyze the difference of the computed vs. ground truth target point positions in the *intra-op* image. The simulation framework provides both ground truth and computed deformation fields for the full organ volume, allowing the expected TRE to be assessed in any target region.

III. Results and Discussion

All simulation software components were built by using freely available libraries and tools. The Insight Segmentation and Registration Toolkit (ITK, www.itk.org) and the Visualization Toolkit (VTK, www.vtk.org) were used for processing image and mesh data, Netgen for mesh generation, and FEBio for FEM solving. We chose widely used standard file formats for storing all input data, as well as intermediate and final results, in order to be compatible with third party software one may want to use for visualization and data analysis.

All the processing steps were implemented as independent executables. Wherever it was possible, we defined a 3D Slicer (www.slicer.org) compatible command-line interface, to allow interactive setting of inputs, running the processing step, and visualizing results – through a graphical user interface. For batch processing mode, to generate a large number of simulation results, we wrote a TCL (www.tcl.tk) script that calls the executables with randomized parameters.

The full source code is available in a repository at the following URL: *git://github.com/lassoan/DefRegEval.git*

The average execution time of a complete simulation cycle was less than 3 minutes on a regular desktop computer (Intel Core2 duo processor running at 2.40GHz). This enables running a large number of simulation cases for parameter exploration and optimization with moderate computing resources.

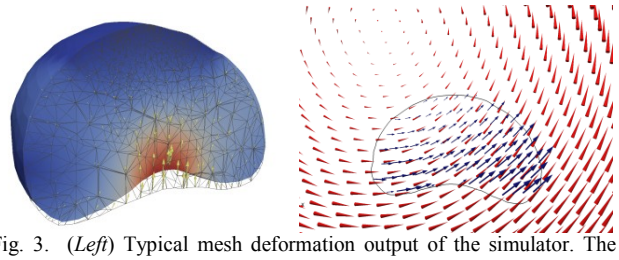

Fig. 3. (*Left*) Typical mesh deformation output of the simulator. The *pre-op* mesh is represented as wireframe, the *intra-op* mesh is shown as a solid surface. (*Right*) Visualization of the non-rigid ground truth deformation field (arrows) and a matching deformation field computed by a rigid registration algorithm (cones) in response to a lateral-anterior direction deforming force.

The simulator provides detailed ground-truth geometry information in surface mesh, volumetric mesh, and segmented image format. A typical volumetric mesh and its

deformation field are shown on Fig. 3(*Left*). Detailed ground truth *pre-op* to *intra-op* deformation information is also available for each node of the mesh and for each voxel of the image. The deformation information reconstructed by the registration algorithm is stored in the same format as the ground truth, making it easy to compare these two pieces of information. A typical example is shown in Fig. 3(*Right*).

A. Evaluation of using a rigid registration algorithm for compensating non-rigid organ deformation

Speed, robustness, and simplicity make rigid registration algorithms a favorable choice for interventional use. However, during prostate needle biopsy procedures the target organ is often non-rigidly deformed.

We used the simulation framework to get detailed information about how much TRE we expect in response to endorectal coil pressure on the prostate. Specifically, what is the spatial distribution of the error, what is the registration error magnitude in case of moderate (2-4mm) and large (4-8mm) patient motion, how the error depends on the direction of the deforming force. The clinically permissible total error is about 3mm (clinically significant size of prostate cancer foci), therefore, the maximum permissible TRE is maximum 3mm (preferably less, because there are other error sources that contribute to the total error).

To get an answer for these questions, we defined 3 simulation groups: A. moderate deformation in response to anterior direction force, B. moderate deformation in response to a lateral-anterior direction force (45 degrees difference compared to group A), C. large dislocation due to anterior direction force.

We executed 100 simulation cases for each group, by setting fixed force parameters while randomly perturbing the prostate shape (by varying the weights by ±20%) and simulating a random segmentation error (±1mm at near two hard-to-segment areas: the prostate apex and base). We composed a max. TRE from all the individual TRE volumes with voxel values corresponding to the highest TRE magnitude at that position in all the volumes in that group. This volume gives the spatial distribution of the maximum TRE. Maximum TRE magnitude histogram for each group are shown in Fig. 4.

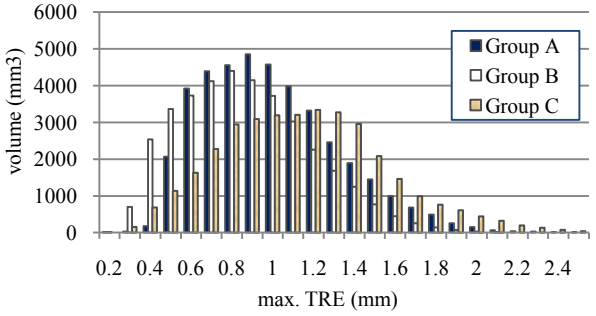

Fig. 4. Maximum TRE distribution for the 3 studied groups.

TABLE I
RANGE OF MAXIMUM DISLOCATION AND TRE VALUES IN THE WHOLE PROSTATE VOLUME

Group	Force direction	Max. dislocation range[a]	Max. TRE range[a]
A	Anterior	1.9 – 6.9 mm	0.6 – 1.5 mm
B	Lateral+Anterior	3.3 – 11.9 mm	0.5 – 1.6 mm
C	Anterior	2.5 – 7.2 mm	0.6 – 1.9 mm

[a]5% to 95% percentile

Similarly to the max. TRE volume, a max. dislocation volume is composed that contains the maximum dislocation magnitude found at each voxel position over all the simulation cases in the group. A comparison of the maximum dislocation and TRE for each group is shown in Table 1.

The above results show that rigid registration can effectively compensate the motion and non-rigid deformation of the prostate, as dislocations up to 12 mm result in less than 2 mm TRE and the TRE had a non-uniform spatial distribution. Near the prostate boundary the TRE magnitude was several times bigger than in the central region. The direction of the deforming force did not seem to affect the resulting TRE, although it almost doubled the dislocation. This phenomenon can be explained by studying the deformation field (Fig. 3*(Right)*.) During lateral-anterior pushing the prostate is more rotated than compressed/deformed, which does not lead to large TRE because and rigid registration can effectively compensate rigid transformations. In all, the simulator functioned as designed and provided useful answer in an important clinical problem.

References

[1] V. Karnik, A. Fenster, J. Bax, D. Cool, *et al*., "Assessment of registration accuracy in three-dimensional transrectal ultrasound images of prostates," SPIE Medical Imaging, Visualization, Image-guided Procedures and Modeling 7625, (2010)

[2] H. Xu, A. Lasso, S. Vikal, P. Guion, *et al*., "Accuracy validation for MRI-guided robotic prostate biopsy," SPIE Medical Imaging, Visualization 2010, Image-guided Procedures and Modeling 7625, (2010)

[3] S. Misra, K. J. Macura, K. T. Ramesh, and A. M. Okamura, "The importance of organ geometry and boundary constraints for planning of medical interventions," Medical Engineering & Physics 31(2), 195-206 (2009)

[4] O. Goksel, S. E. Salcudean, and S. P. DiMaio, "3D simulation of needle tissue interaction with application to prostate brachytherapy," Computer Aided Surgery, 11(6), 279-288 (2006)

[5] P. Courtis, A. Samani, "Detecting mechanical abnormalities in prostate tissue using FE-based image registration," Med Image Comp Comput Assist Interv. 2007;10(Pt 2):244-51.

[6] J. M. Hensel, C. Ménard, P. W. M. Chung, *et al*., "Development of multiorgan finite element-based prostate deformation model enabling registration of endorectal coil magnetic resonance imaging for radiotherapy planning," Int. J. Radiation Oncology Biol. Phys. 68:1522-1528 (2007)

[7] Huai-Ping Lee, Ming Lin, and Mark Foskey, "Physically-Based validation of deformable medical image registration," Med Image Comput Comput Assist Interv.,11(Pt 2):830-8 (2008)

[8] A. Tsai, *et al*., "A shape-based approach to the segmentation of medical imagery using level sets," IEEE Trans. on Medical Imaging 22(2), 137-154 (2003)

[9] M. E. Leventon, W. E. L. Grimson, and O. Faugeras, "Statistical shape influence in geodesic active contours," Proc. the IEEE Computer Society Conference on Computer Vision and Pattern Recognition, 316-323 (2000)